A NONLINEAR DIGITAL MODEL OF THE EMS VCS3 VOLTAGE-CONTROLLED FILTER

Marco Civolani
University of Verona
Dipartimento di Informatica
15 Strada Le Grazie
Verona 37134, Italy
marco.civolani@gmail.com

Federico Fontana
University of Verona
Dipartimento di Informatica
15 Strada Le Grazie
Verona 37134, Italy
federico.fontana@univr.it

ABSTRACT

This article presents a nonlinear discrete-time model of the EMS VCS3 voltage-controlled filters. The development of the model is based on the study of the filter circuitry and its behavior in the time domain. From this circuitry a system of nonlinear differential equations has been derived describing the dynamics in regime of large signals. The digital implementation of the filter is based on a numerical approximation of those equations. The resulting Matlab model has been compared with a structurally identical simulation running under PSpice. Finally, a real-time realization of the VCF has been implemented under the Pure Data processing environment.

1. ANALOG SYSTEM

The *Voltage-Controlled for Studio with 3 oscillators* (VCS3) was an analog modular monophonic synthesizer designed by David Cockerell in 1969 and produced by Peter Zinovieff for the Electronic Music Studio Ltd in London. The voltage-controlled filter (VCF) that was embedded in this synthesizer used junction diodes as variable-resistance components to control the cutoff frequency.

The circuit is based on a ladder structure, that is very similar to that implemented in the renowned Moog VCF [1, 2, 3, 4, 5]. The main difference between the two circuits resides in the fact that the latter uses bipolar junction transistors (BJT) instead of diodes to control the cutoff frequency. Notes for a discrete-time implementation of this structure have been drawn by Borin [6].

Figure 1 shows the circuit of the VCF. It is basically a *differential amplifier* loaded with a diode-capacitor network, where the diodes act as current-controlled resistors. Their resistance in fact determines the filter cutoff frequency, and is related to the control current I_0 imposed by the BJT Q4 which acts as a current generator controlled by the voltage V_{CV}. The polarization of the diodes is ensured by Q3, which provides 9V at the top of the ladder: this allows the current to flow in the two branches as indicated in Figure 1.

The VCF features also a feedback circuit whose variable resistance can induce a gain ranging from 0 to about 10 (as indicated on the control panel of the synthesizer). This circuit is based on the OP-AMP U1 whose output is sent to the base of Q2 (thus closing the feedback loop), as well as to the filter output. To realize the feedback, the voltage across C4 (which is the output of the filter in open-loop mode) is sent at the inputs of U1 through a first-order highpass filter (the RC cell constituted by C7 and R7 on one branch, and by C8 and R8 on the other one) to eliminate the DC offset caused by the polarization voltages present in the signal. The same feature is realized by C5 and C6. The three diodes D9, D11 and D13 and, correspondingly, D10, D12 and D14, act as two *pull-up* current-controlled resistors. Indeed they could be substituted with two resistors, but this solution would limit the efficiency of the control current I_0 in varying the cutoff frequency, furthermore it would linearize the whole circuit and consequently change its peculiar sound.

2. DERIVATION OF THE MODEL

First, a linearized open-loop version of the circuit has been modeled by disconnecting the feedback: in this *open-loop* version, the diodes were substituted by equivalent *differential resistances* and the two BJTs Q1 and Q2 were substituted by simplified versions of the *Hybrid-π* model (also known as *trans-conductance model*) [7]. The resulting circuit describes the open loop filter in regime of small signals.

Then, the nonlinearities have been taken into account. Diodes were modeled with an exponential voltage-to-current characteristics that describes their behavior under conditions of direct polarization. BJTs were modeled with the *Ebers-Moll* model [7]. A model for the open-loop VCF has been so achieved, capable of describing the system behavior in regime of large signals.

Last, the variable gain feedback circuit has been included in the nonlinear model. As it usual for this type of amplifiers, the OP-AMP U1 has been modeled under the assumption of linear behavior.

3. NONLINEAR MODEL OF THE FILTER IN OPEN LOOP

It is possible to assume that the diodes in the two branches of the ladder are always directly polarized. Their behavior in the large signals domain is therefore described with good approximation by Eq. (1):

$$i = I_{\text{inv}} \left(e^{\frac{v}{\eta V_T}} - 1 \right), \tag{1}$$

Where I_{inv} is the diode inverse polarization current, which usually amounts to some nA and η is the *emission coefficient*, a parameter related to the diode model: for the 1N4148 (used in the VCF), $\eta = 1.836$. Furthermore, V_T is the so-called *thermal voltage*: $V_T = kT/q \approx 0.026$ mV at 25°C, where $q = 1,60206^{-19}$C is the fundamental electric charge unit, k is the Boltzmann constant, T is the temperature measured in Kelvin degrees, and V_T is the so-called *thermal voltage*. The following equation can straightfor-

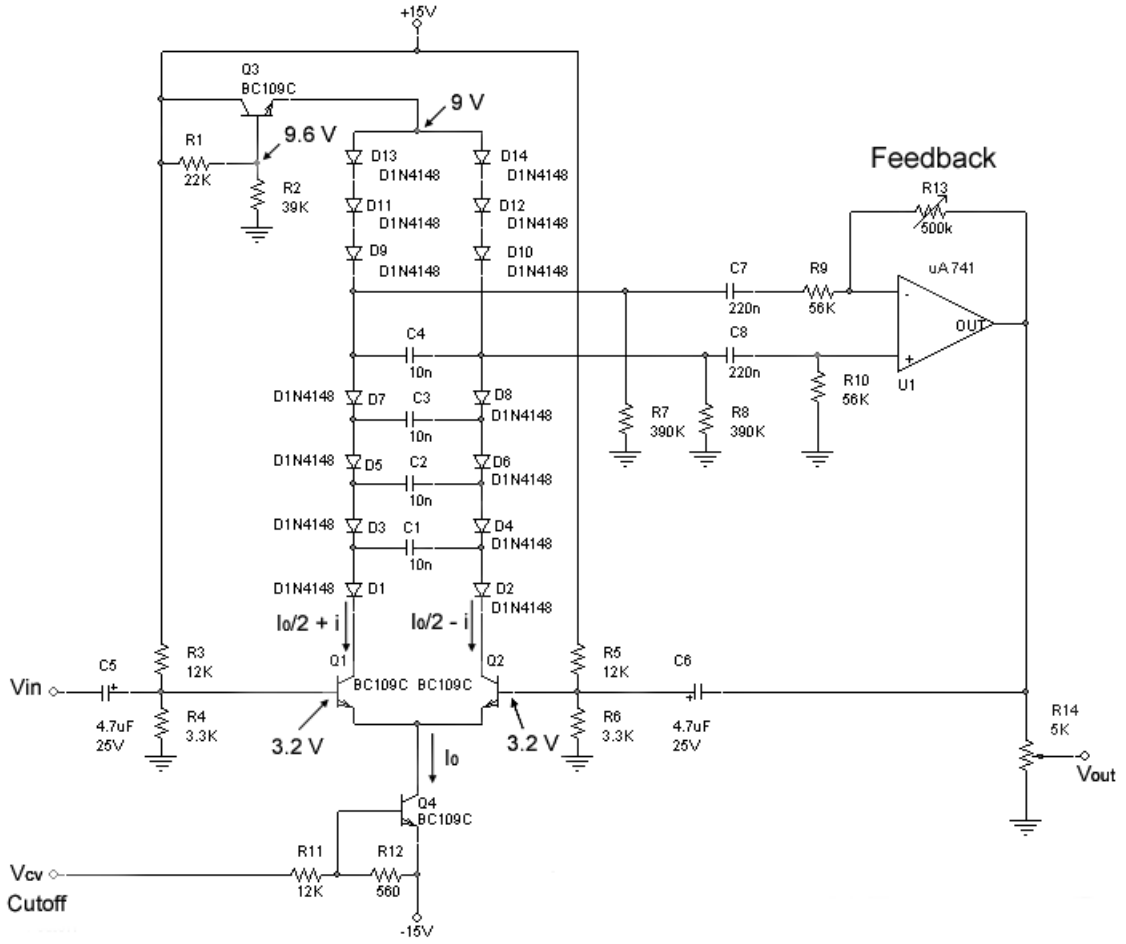

Figure 1: *Schematic of the EMS VCS3 VCF circuitry.*

wardly be derived from Eq. (1):

$$v = \eta V_T \ln\left(\frac{i}{I_{\text{inv}}}\right). \tag{2}$$

The transistors Q1 and Q2 have been modeled with the *Ebers-Moll* model which is able to describe their nonlinear behavior in active mode with good approximation. The Ebers-Moll model describes the NPN BJTs in the form of an equivalent circuit, as shown in Figure 2. The two diodes in the model represent the base-to-emitter and base-to-collector junctions. The two current sources quantify minor transports of charge through the base region, and depend on the intensity of the current flowing through each diode. The equations which characterize the model are the following:

$$I_E = I_{ES}\left(e^{\frac{V_{BE}}{V_T}} - 1\right) \tag{3}$$

$$I_C = \alpha_0 I_{ES}\left(e^{\frac{V_{BE}}{V_T}} - 1\right), \tag{4}$$

where I_E is current at the emitter, I_C is the current at the collector, α_0 is the short circuit current gain in common base configuration (values ranging between 0.980 and 0.998), I_{ES} is the inverse current of the diode between the base and the emitter, and finally V_{BE}

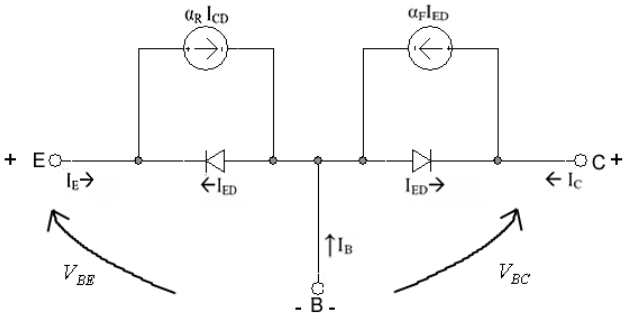

Figure 2: *The NPN BJT equivalent circuit provided by the Ebers-Moll model.*

is the voltage between the base and the emitter. The current gain β_0 can be considered to be very high and, thus, approximating infinity. Moreover, by keeping in mind that:

$$\beta_0 = \frac{\alpha_0}{1-\alpha_0} \longleftrightarrow \alpha_0 = \frac{\beta_0}{1+\beta_0}, \tag{5}$$

then α_0 can be approximatively considered equal to 1. Now, since:

$$\alpha_0 = I_C/I_E \quad \text{and} \quad \beta_0 = I_C/I_B \tag{6}$$

it can be deduced that the base current can be considered equal to zero, while the emitter current is equal to that flowing along the collector. Holding these assumptions, the fundamental equation useful to describe the behavior of a BJT with the *Ebers-Moll* model is Eq. (3).

In order to apply the model to the open-loop VCF, it is necessary to understand how it deals with the circuit at the base of the VCF itself, i.e. the long-tailed pair differential amplifier based on the BJTs Q1 and Q2. Thus, it is useful to analyze the circuit part shown in Figure 3. By applying Eq. (3) to Q1 and Q2 respectively,

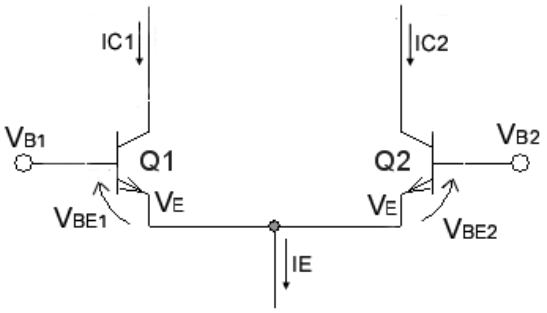

Figure 3: *The Ebers-Moll model in the long-tailed pair differential amplifier.*

the two following equations can be derived:

$$\begin{aligned} i_{C1} &= I_{ES1}\left(e^{\frac{v_{BE1}}{V_T}} - 1\right) \approx I_{ES1}\left(e^{\frac{v_{BE1}}{V_T}}\right) \\ i_{C2} &= I_{ES2}\left(e^{\frac{v_{BE2}}{V_T}} - 1\right) \approx I_{ES2}\left(e^{\frac{v_{BE2}}{V_T}}\right) \end{aligned} . \tag{7}$$

Thus:

$$v_{BE1} = V_T \ln\left(\frac{i_{C1}}{I_{ES1}}\right) \text{ and } \quad v_{BE2} = V_T \ln\left(\frac{i_{C2}}{I_{ES2}}\right). \tag{8}$$

Now, it is interesting to study the behavior of a long-tailed pair differential amplifier taking the voltage between the input terminals as an input signal. The two following relations have to be considered:

$$v_{BE2} - v_{BE1} = V_T \ln\left(\frac{i_{C2} \cdot I_{ES1}}{i_{C1} \cdot I_{ES2}}\right). \tag{9}$$

Assuming that the inverse base-to-emitter current in Q1 has the same value of the one in Q2, i.e. $I_{ES1} = I_{ES2}$ (for example, by the adoption of a matched-pair of transistors), it can be obtained that:

$$v_{BE2} - v_{BE1} = V_T \ln\left(\frac{i_{C2}}{i_{C1}}\right). \tag{10}$$

Now, since:

$$v_{BE2} - v_{BE1} = (v_{B2} - v_E) - (v_{B1} - v_E),$$

by taking into account that the two emitters are directly connected together, it follows that:

$$v_{BE2} - v_{BE1} = v_{B2} - v_{B1} \tag{11}$$

and, by calculating the exponential for both the members of Eq. (10), it can be obtained that:

$$e^{\frac{v_{B2}-v_{B1}}{V_T}} = \frac{i_{C2}}{i_{C1}}. \tag{12}$$

Thus, as suggested in [4]:

$$i_E = i_{C1} + i_{C2} = i_{C1} + i_{C1} e^{\frac{v_{B2}-v_{B1}}{V_T}}, \tag{13}$$

which leads to:

$$i_{C1} = \frac{i_E}{1 + e^{\frac{v_{B2}-v_{B1}}{V_T}}}.$$

This formula can be rewritten as:

$$\begin{aligned} i_{C1} &= \frac{2 i_E}{2\left(1+e^{\frac{v_{B2}-v_{B1}}{V_T}}\right)} \\ &= \frac{i_E}{2}\left(\frac{1+1+e^{\frac{v_{B2}-v_{B1}}{V_T}} - e^{\frac{v_{B2}-v_{B1}}{V_T}}}{1+e^{\frac{v_{B2}-v_{B1}}{V_T}}}\right) \\ &= \frac{i_E}{2}\left(1 + \frac{1-e^{\frac{v_{B2}-v_{B1}}{V_T}}}{1+e^{\frac{v_{B2}-v_{B1}}{V_T}}}\right). \end{aligned}$$

Now, since:

$$\tanh x = \frac{e^x - e^{-x}}{e^x + e^{-x}} = \frac{e^{2x} - 1}{e^{2x} + 1}$$

by making the necessary substitutions, it can be derived that:

$$\begin{aligned} i_{C1} &= \frac{i_E}{2}\left[1 - \tanh\left(\frac{v_{B2}-v_{B1}}{2V_T}\right)\right] \\ &= \frac{i_E}{2}\left[1 + \tanh\left(\frac{v_{B1}-v_{B2}}{2V_T}\right)\right] \end{aligned} \tag{14}$$

and

$$\begin{aligned} i_{C2} = i_E - i_{C1} &= i_E - \frac{i_E}{2}\left[1 + \tanh\left(\frac{v_{B1}-v_{B2}}{2V_T}\right)\right] \\ &= \frac{i_E}{2}\left[1 - \tanh\left(\frac{v_{B1}-v_{B2}}{2V_T}\right)\right]. \end{aligned} \tag{15}$$

The last two equations have been exploited in order to obtain the system of nonlinear differential equations constituting the model of the VCF in regime of large signals: the nonlinear open loop filter is shown in Figure 4. Since the three diodes D9, D11 and D13 are in series, they are traversed by the same current, furthermore the voltage pull-down is the same for each of them. So:

$$V_{D_9} + V_{D_{11}} + V_{D_{13}} = 3V_{D_9}.$$

D10, D12 and D14 undertake the same effect:

$$V_{D_{10}} + V_{D_{12}} + V_{D_{14}} = 3V_{D_{10}}.$$

The application of the Kirchhoff law for voltages on the circuit in Figure 4 leads to the following system of equations:

$$\begin{cases} v_{D_3} + v_{C_2} - v_{D_4} - v_{C_1} &= 0 \\ v_{D_5} + v_{C_3} - v_{D_6} - v_{C_2} &= 0 \\ v_{D_7} + v_{C_4} - v_{D_8} - v_{C_3} &= 0 \\ 3v_{D_9} - 3v_{D_{10}} - v_{C_4} &= 0 \end{cases}, \tag{16}$$

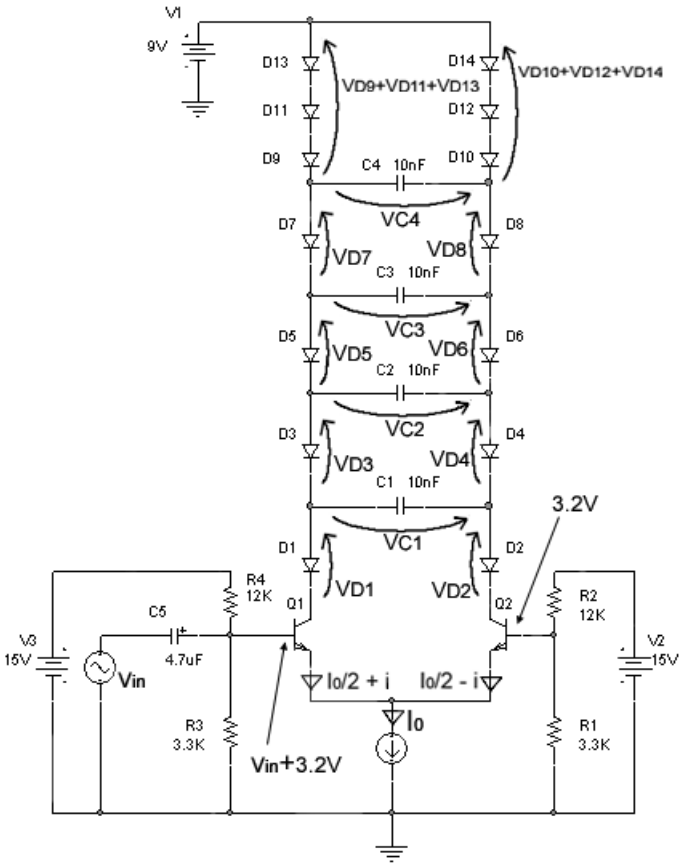

Figure 4: *The nonlinear open loop version of the VCF.*

which, with the application of logarithms, and considering that $C_1 = C_2 = C_3 = C_4 = C$, after some algebraic manipulations can be rewritten as:

$$\begin{cases} \dot{v}_{C_1} = \frac{I_0}{2C} \frac{1-e^{\frac{v_{C_1}-v_{C_2}}{\gamma}}}{1+e^{\frac{v_{C_1}-v_{C_2}}{\gamma}}} + \frac{i}{C} \\ \dot{v}_{C_2} = \frac{I_0}{2C} \left(\frac{1-e^{\frac{v_{C_1}-v_{C_2}}{\gamma}}}{1+e^{\frac{v_{C_1}-v_{C_2}}{\gamma}}} + \frac{1-e^{\frac{v_{C_2}-v_{C_3}}{\gamma}}}{1+e^{\frac{v_{C_2}-v_{C_3}}{\gamma}}} \right) \\ \dot{v}_{C_3} = \frac{I_0}{2C} \left(\frac{1-e^{\frac{v_{C_2}-v_{C_3}}{\gamma}}}{1+e^{\frac{v_{C_2}-v_{C_3}}{\gamma}}} + \frac{1-e^{\frac{v_{C_3}-v_{C_4}}{\gamma}}}{1+e^{\frac{v_{C_3}-v_{C_4}}{\gamma}}} \right) \\ \dot{v}_{C_4} = \frac{I_0}{2C} \left(\frac{1-e^{\frac{v_{C_3}-v_{C_4}}{\gamma}}}{1+e^{\frac{v_{C_3}-v_{C_4}}{\gamma}}} + \frac{1-e^{\frac{v_{C_4}}{3\gamma}}}{1+e^{\frac{v_{C_4}}{3\gamma}}} \right) \end{cases}, \quad (17)$$

where γ is an auxiliary quantity defined in order to keep the notation readable:

$$\gamma \triangleq \eta \cdot V_T \approx 1.836 \cdot 0.026 \approx 0.048, \quad (18)$$

and the current i is due to the application of the input voltage v_{in} at the base of Q1. In order to obtain a set of equations which relates

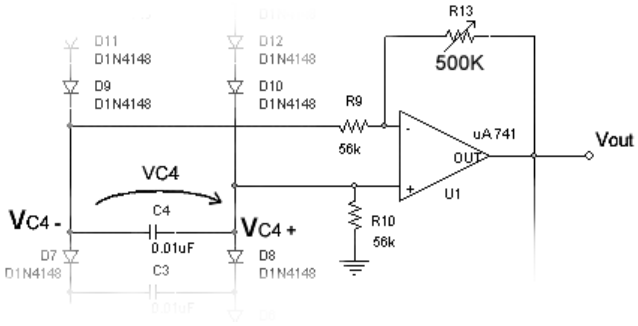

Figure 5: *The differential amplifier used in the VCF as variable gain feedback circuit.*

v_{in} with the output v_{C_4}, the substitution of (14) is necessary:

$$\begin{aligned} i &= \frac{I_0}{2}\left[1+\tanh\left(\frac{v_{in}+3.2V-3.2V}{2V_T}\right)\right] \\ &= \frac{I_0}{2}\left[1+\tanh\left(\frac{v_{in}}{2V_T}\right)\right]. \end{aligned}$$

Hence:

$$\begin{cases} \dot{v}_{C_1} = \frac{I_0}{2C} \frac{1-e^{\frac{v_{C_1}-v_{C_2}}{\gamma}}}{1+e^{\frac{v_{C_1}-v_{C_2}}{\gamma}}} + \frac{I_0}{2C}\left(1+\tanh\left[\frac{v_{in}}{2V_T}\right]\right) \\ \dot{v}_{C_2} = \frac{I_0}{2C} \left(\frac{1-e^{\frac{v_{C_1}-v_{C_2}}{\gamma}}}{1+e^{\frac{v_{C_1}-v_{C_2}}{\gamma}}} + \frac{1-e^{\frac{v_{C_2}-v_{C_3}}{\gamma}}}{1+e^{\frac{v_{C_2}-v_{C_3}}{\gamma}}} \right) \\ \dot{v}_{C_3} = \frac{I_0}{2C} \left(\frac{1-e^{\frac{v_{C_2}-v_{C_3}}{\gamma}}}{1+e^{\frac{v_{C_2}-v_{C_3}}{\gamma}}} + \frac{1-e^{\frac{v_{C_3}-v_{C_4}}{\gamma}}}{1+e^{\frac{v_{C_3}-v_{C_4}}{\gamma}}} \right) \\ \dot{v}_{C_4} = \frac{I_0}{2C} \left(\frac{1-e^{\frac{v_{C_3}-v_{C_4}}{\gamma}}}{1+e^{\frac{v_{C_3}-v_{C_4}}{\gamma}}} + \frac{1-e^{\frac{v_{C_4}}{3\gamma}}}{1+e^{\frac{v_{C_4}}{3\gamma}}} \right) \end{cases}. \quad (19)$$

The nonlinear system (19) describes the behavior of the VCF when in open loop.

4. CLOSING THE LOOP

As previously said, the VCF features also a variable gain feedback circuit based on the OP-AMP U1, which has been modeled assuming linearity. In particular, this part of the circuit can be described by applying the superposition principle to the circuit in Figure 5, thus obtaining the following input-output relationship:

$$v_{out} = v_{C_{4+}} \frac{R_9 + R_{13}}{R_9} - v_{C_{4-}} \frac{R_{13}}{R_9}. \quad (20)$$

Now, considering what happens to the currents and voltages involved in the long-tailed pair differential amplifier, and applying these considerations to the branches of the ladder based on Q1 and Q2, it can be figured out that:

$$v_{C_{4+}} = -v_{C_{4-}}.$$

Hence:

$$v_{C_4} = v_{C_{4+}} - v_{C_{4-}} = 2v_{C_{4+}}.$$

Thus, Eq. (20) can be rewritten as:

$$\begin{aligned} v_{out} &= v_{C_{4+}} \frac{R_9 + R_{13}}{R_9} + v_{C_{4+}} \frac{R_{13}}{R_9} \\ &= v_{C_{4+}} + 2v_{C_{4+}} \frac{R_{13}}{R_9} \\ &= \frac{v_{C_4}}{2} + v_{C_4} \frac{R_{13}}{R_9}. \end{aligned} \tag{21}$$

The term R_{13}/R_9 represents the *gain* of the feedback circuit. Now, since R13 varies from 0 Ω to 500 kΩ and R9 = 56 kΩ, the gain varies from 0 to about 10. Considering Eq. (14), then relation (21) can be directly substituted in the system (19) obtaining:

$$\begin{cases} \dot{v}_{C_1} = \frac{I_0}{2C} \left(\frac{1-e^{\frac{v_{C_1}-v_{C_2}}{\gamma}}}{1+e^{\frac{v_{C_1}-v_{C_2}}{\gamma}}} + \tanh\left[\frac{v_{in} - \frac{v_{C_4}}{2} - v_{C_4}\frac{R_{13}}{R_9}}{2V_T} \right] + 1 \right) \\ \dot{v}_{C_2} = \frac{I_0}{2C} \left(\frac{1-e^{\frac{v_{C_1}-v_{C_2}}{\gamma}}}{1+e^{\frac{v_{C_1}-v_{C_2}}{\gamma}}} + \frac{1-e^{\frac{v_{C_2}-v_{C_3}}{\gamma}}}{1+e^{\frac{v_{C_2}-v_{C_3}}{\gamma}}} \right) \\ \dot{v}_{C_3} = \frac{I_0}{2C} \left(\frac{1-e^{\frac{v_{C_2}-v_{C_3}}{\gamma}}}{1+e^{\frac{v_{C_2}-v_{C_3}}{\gamma}}} + \frac{1-e^{\frac{v_{C_3}-v_{C_4}}{\gamma}}}{1+e^{\frac{v_{C_3}-v_{C_4}}{\gamma}}} \right) \\ \dot{v}_{C_4} = \frac{I_0}{2C} \left(\frac{1-e^{\frac{v_{C_3}-v_{C_4}}{\gamma}}}{1+e^{\frac{v_{C_3}-v_{C_4}}{\gamma}}} + \frac{1-e^{\frac{v_{C_4}}{3\gamma}}}{1+e^{\frac{v_{C_4}}{3\gamma}}} \right) \end{cases} \tag{22}$$

The system (22) describes the VCF in regime of large signals.

5. SIMULATIONS

Matlab simulations using explicit fourth-order Runge-Kutta have been employed to integrate system (22) in the discrete domain. For what concerns the integration algorithm, system (22) can be written as

$$\dot{y} = F(t, v_C)$$

which leads to the usual representation of the method:

$$\begin{aligned} K_0 &= hF\left(t_i, v_{C_i}\right) \\ K_1 &= hF\left(t_i + \tfrac{h}{2}, v_{C_i} + \tfrac{K_0}{2}\right) \\ K_2 &= hF\left(t_i + \tfrac{h}{2}, v_{C_i} + \tfrac{K_1}{2}\right) \\ K_3 &= hF\left(t_i + h, v_{C_i} + K_2\right) \end{aligned} \tag{23}$$

Where t_i is the *i-th* integration step and v_{C_i} is a 4×1 vector representing the voltages across the four capacitors at the *i-th* integration step. These voltages can thus be updated as follows:

$$v_{C_{i+1}} = v_{C_i} + \frac{1}{6}\left(K_0 + 2K_1 + 2K_2 + K3\right) \tag{24}$$

A fixed-point iteration scheme has then been implemented in order to find the exact value of v_{C_4} (under a chosen threshold), for each integration step, as required by system (22).

Figures 6-8 show simulation results coming out when linearly sweeping sinusoids with fixed amplitude from 20 Hz to 8 kHz at different input dynamics, along 4 s simulation time and using a sampling frequency $F_s = 88.2$ kHz. In every figure the upper plot shows the waveform of the output signal, whereas the lower spectrogram depicts the evolution of the magnitude spectrum in the corresponding simulation. The upper plots in every figure show the frequency dependence of the lowpass characteristics: the amplitude of the output signal decreases with time, while frequency grows up. Furthermore by comparing the spectrograms computed for different dynamics it becomes evident that larger amplitudes lead to higher harmonic distortion. Figures 9-13 investigate the effects of feedback, using similar parameterizations of the circuit. As it can be seen in the previously mentioned Figures, the model suffers from aliasing: this particular problem will be taken into account in the next refinings of the model. Finally, Figure 14 shows the waveform and the spectrogram of a drum loop used as test sample; Figures 15-17 show some simulation results obtained by injecting this loop into the filter with different setups.

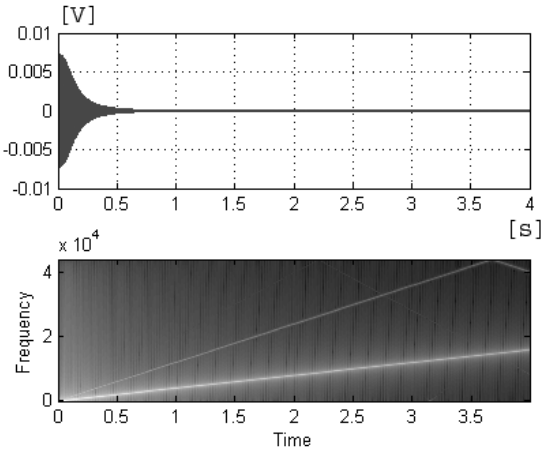

Figure 6: *20 Hz to 8 kHz linear sinusoidal sweep with 10 mV amplitude peak. $I_0 = 30$ μA, without feedback ($R_{13} = 0$).*

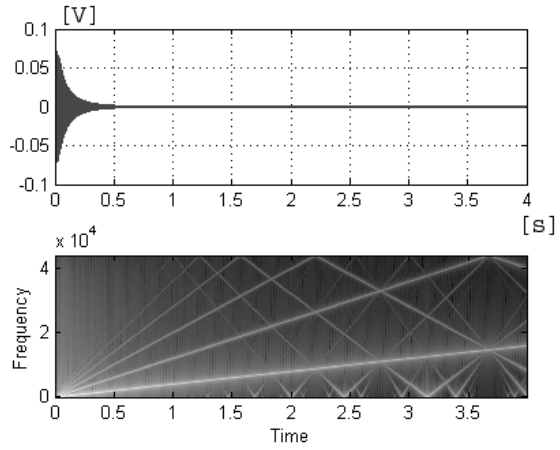

Figure 7: *20 Hz to 8 kHz linear sinusoidal sweep with 100 mV amplitude peak. $I_0 = 30$ μA, without feedback ($R_{13} = 0$).*

The closed-loop nonlinear VCF was also analyzed using offline PSpice software simulation as a reference: several sinusoids

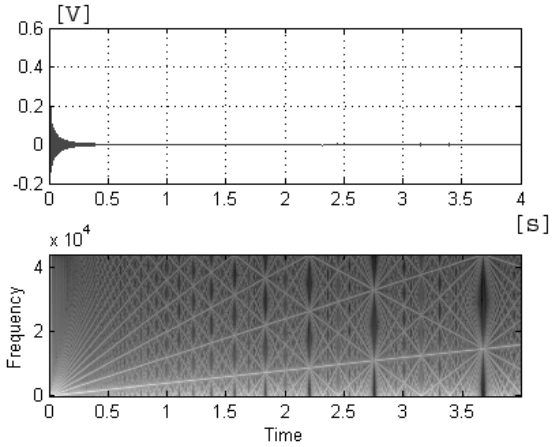

Figure 8: *20 Hz to 8 kHz linear sinusoidal sweep with 1 V amplitude peak. $I_0 = 30$ μA, without feedback.*

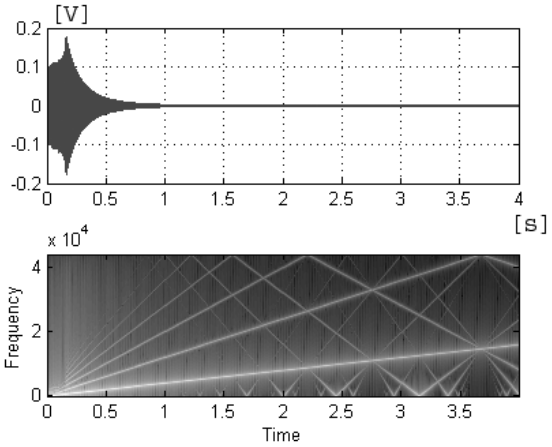

Figure 10: *20 Hz to 8 kHz linear sinusoidal sweep with 100 mV amplitude peak. $I_0 = 30$ μA, feedback gain $R_{13}/R_9 = 5$.*

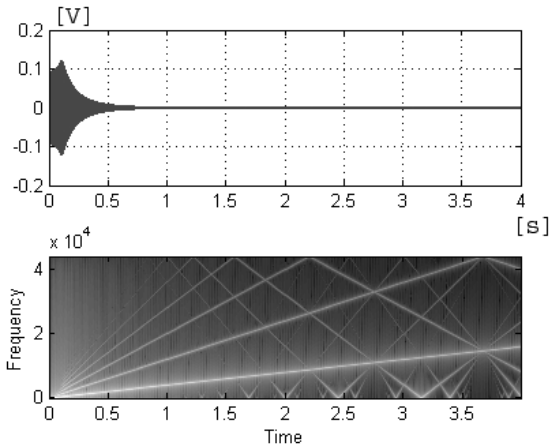

Figure 9: *20 Hz to 8 kHz linear sinusoidal sweep with 100 mV amplitude peak. $I_0 = 30$ μA, feedback gain $R_{13}/R_9 = 2$.*

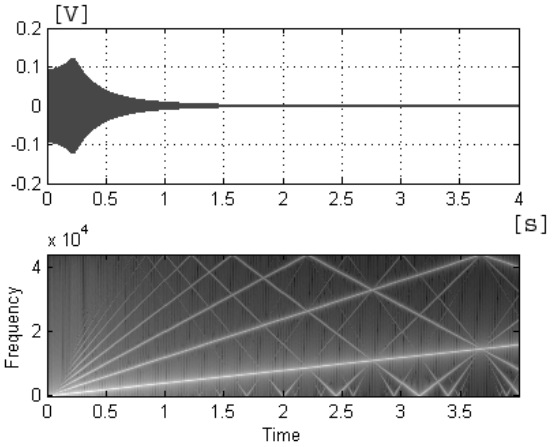

Figure 11: *20 Hz to 8 kHz linear sinusoidal sweep with 100 mV amplitude peak. $I_0 = 60$ μA, feedback gain $R_{13}/R_9 = 2$.*

with fixed amplitude and different frequency have been injected in the PSpice model as well as in the Matlab model. The qualitative comparison between the waveforms of the respective outputs outlined a good coherence of the two models: a relevant prove of that, is the comparison between the RMS values of the outputs, shown in Table 1. The results were very similar for almost all the inputs used in the tests except for differences mainly due to the fact that the proposed model does not account for the dc-cut capacitors C5, C6, C7, and C8 (see section 1). These high-pass blocks in fact, while completely blocking components below 20 Hz, obviously filter the signal also above that frequency. Such effects should have minor perceptual impact, however high-pass filtering blocks will be introduced in a further version of the model.

Finally the model has been implemented on a 2.0 GHz Core 2 Duo MacBook laptop mounting MacOS X v. 10.4, equipped with the Pure Data real time simulation environment, in the form of a C *external*. Figure 18 shows a snapshot of the resulting Pure Data *patch* realizing the VCF. In such an environment the constraint of real time has been checked depending on the number of fixed-point iterations needed by the system to converge to a solution satisfying an accepted threshold of accuracy. This number in fact must be low enough, in order to prevent the formation of artifacts that become audible when the computational burden overcomes the performance of the computer. A non systematic campaign of tests has been conducted using different kinds of input signals, such as sawtooth and square waves, noise, different kinds of audio samples, etc. By setting a threshold of accuracy on v_{C_4} equal to 10 mV, the number of iterations needed to stay below that threshold was never larger than 2. This means that the nonlinear implicit system is in general well-conditioned for fixed-point iteration, and that more accurate solutions can be easily achieved by scaling down the threshold with the performance of the computer at hand.

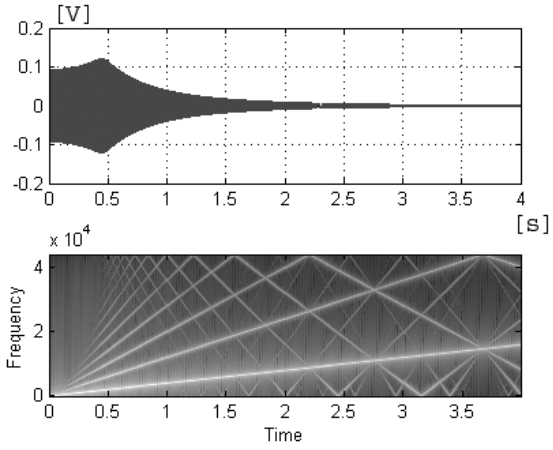

Figure 12: *20 Hz to 8 kHz linear sinusoidal sweep with 100 mV amplitude peak.* $I_0 = 120$ *μA, feedback gain* $R_{13}/R_9 = 2$.

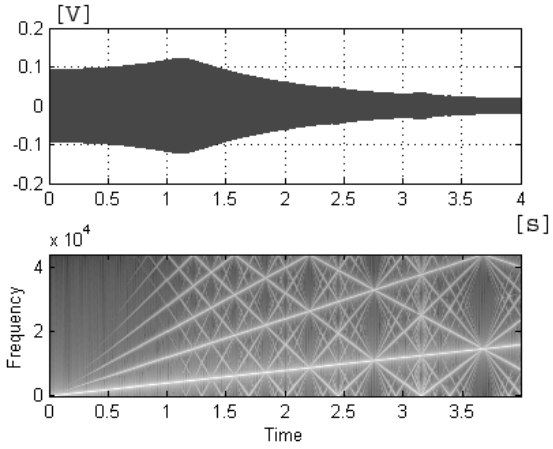

Figure 13: *20 Hz to 8 kHz linear sinusoidal sweep with 100 mV amplitude peak.* $I_0 = 300$ *μA, feedback gain* $R_{13}/R_9 = 2$.

Some sound examples obtained with the real-time Pure Data module of the filter are downloadable at the following URL: *https://mordente.sci.univr.it/samba/Accessible/VCS3Examples*

6. CONCLUSIONS AND FUTURE WORK

This work has presented a digital model of the EMS VCS3 voltage-controlled filter: its circuitry has been modeled in the discrete time using Fourth-order Runge-Kutta, and fixed-point iteration has been successfully implemented to solve the resulting nonlinear implicit numerical system. In this way many structural features that give to this device its particular sound could be simulated with good precision, such as its most evident nonlinear characteristics. Concerning the numerical aspects, traditional and robust numerical recipes have been chosen since they provide accurate enough solutions in this particular case when the discrete components (which are also the most relevant sources of nonlinearity) are supposed to work always in the active region (i.e., in conditions of direct polarization). On the other hand, more expressive, but also computationally demanding models could be used instead in order to obtain a higher grade of fidelity accounting also for other activity regions of the semiconductors.

In addition to that, both the integration and the iteration problem could be recast by keeping into account alternative methods, especially designed for the solution of nonlinear implicit numerical systems arising in presence of delay-free feedback chains [8]. The use of such methods is left to a future implementation of the system.

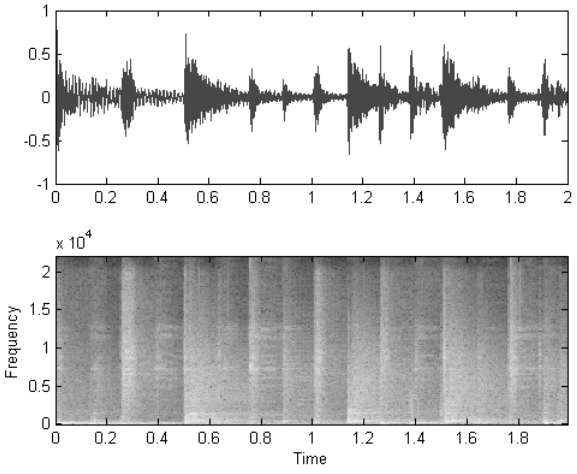

Figure 14: *Drum loop sample with kick drum, snare and hi-hat used for tests.*

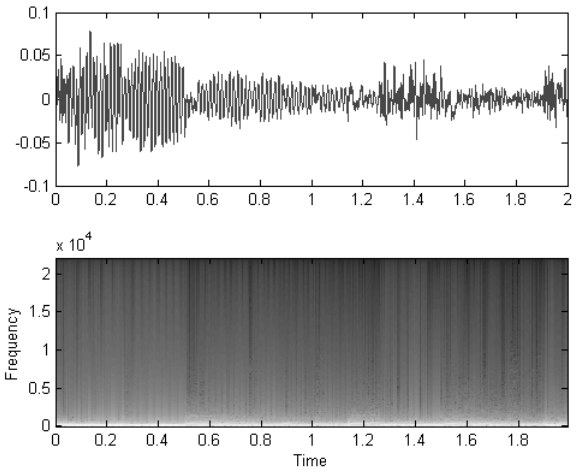

Figure 15: *Output generated with the drum sample of Figure 14 with feedback gain* $R_{13}/R_9 = 1$, $I_0 = 4$ *μA.*

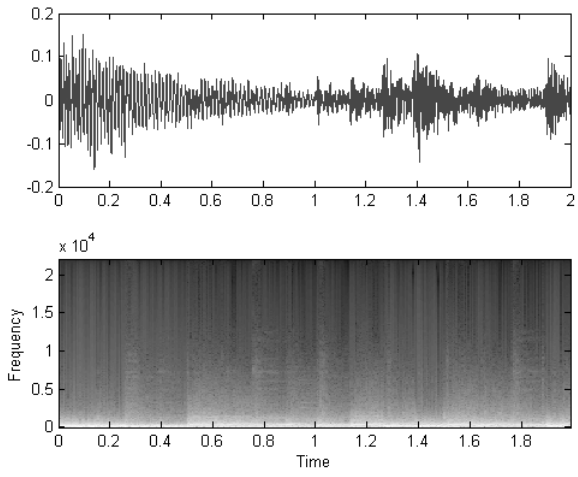

Figure 16: *Output generated with the drum sample of Figure 14 with feedback gain $R_{13}/R_9 = 1$, $I_0 = 10\ \mu A$.*

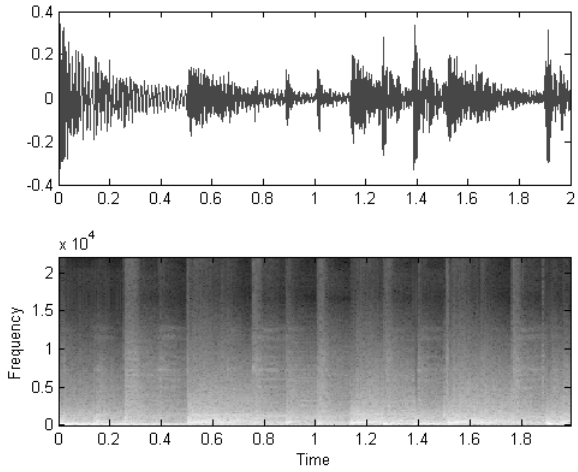

Figure 17: *Output generated with the drum sample of Figure 14 with feedback gain $R_{13}/R_9 = 1$, $I_0 = 40\ \mu A$.*

Frequency (Hz)	Matlab (V RMS)	PSpice (V RMS)
40	0.60	0.63
80	0.63	0.67
160	0.63	0.67
320	0.65	0.69
640	0.60	0.63
1280	0.23	0.23
2560	0.08	0.08

Table 1: *Comparison between RMS values measured at the output of the VCF, respectively simulated using Matlab and PSpice. The input signals were sine waves having different frequencies as shown in the first column, with 1 V peak amplitude, $I_0 = 48\ \mu A$, and feedback gain $R_{13}/R_9 = 2$.*

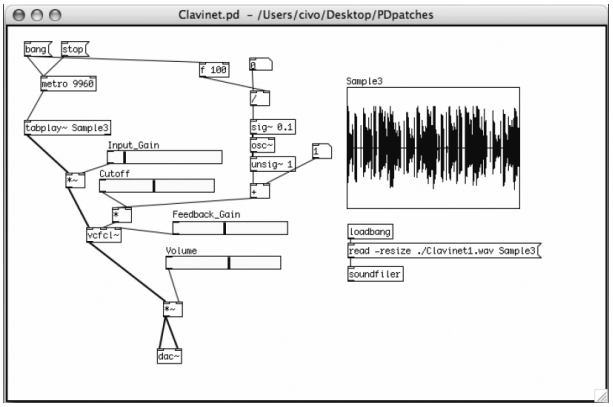

Figure 18: *Pure Data patch of the nonlinear VCF.*

7. REFERENCES

[1] R. A. Moog, "A voltage-controlled low-pass high-pass filter for audio signal processing," in *Audio Engineering Society Convention*. AES, Oct. 1965, Preprint 413.

[2] T. Stilson and J. O. Smith, "Analyzing the Moog VCF with considerations for digital implementation," in *Proc. Int. Computer Music Conf.*, Hong Kong, 1996.

[3] A. Huovilainen, "Nonlinear digital implementation of the moog ladder filter," in *Proc. Conf. on Digital Audio Effects (DAFX-04)*, Naples, Italy, Oct. 2004, pp. 61–64.

[4] T. E. Stinchombe, "Derivation of the transfer function of the moog ladder filter," Web published at http://mysite.wanadoo-members.co.uk/tstinchcombe/synth/Moog_ladder_tf.pdf.

[5] F. Fontana, "Preserving the structure of the moog VCF in the digital domain," in *Proc. Int. Computer Music Conf.*, Copenhagen, Denmark, 27–31 Aug. 2007.

[6] G. Borin, "Appunti sul VCF," Internal Technical Report, 2000, Unpublished.

[7] R. C. Jaeger and T. N. Blalock, *Microelectronic Circuit Design*, McGraw-Hill, New York, 2nd edition, 2004.

[8] F. Fontana and F. Avanzini, "Computation of delay-free nonlinear digital filter networks. application to chaotic circuits and intracellular signal transduction," *IEEE Trans. on Signal Processing*, 2008, Submitted.